Inorg. Chem. **2004**, *43*, 1012–1020

Electrochemical and Spectroelectrochemical Characterization of Ru_2^{4+} and Ru_2^{3+} Complexes under a CO Atmosphere

Karl M. Kadish,*,† Tuan D. Phan,† Lingamallu Giribabu,† Jianguo Shao,† Li-Lun Wang,† Antoine Thuriere,† Eric Van Caemelbecke,†,‡ and John L. Bear*,†

Departments of Chemistry, University of Houston, Houston, Texas 77204-5003, and Houston Baptist University, Houston, Texas 77074-3298

Received September 1, 2003

Eleven different Ru_2^{4+} and Ru_2^{3+} derivatives are characterized by thin-layer FTIR and UV–visible spectroelectrochemistry under a CO atmosphere. These compounds, which were in-situ electrogenerated from substituted anilinopyridine complexes with a Ru_2^{5+} core, are represented as $Ru_2(L)_4Cl$ where L = 2-CH_3ap, ap, 2-Fap, 2,3-F_2ap, 2,4-F_2ap, 2,5-F_2ap, 3,4-F_2ap, 3,5-F_2ap, 2,4,6-F_3ap, or F_5ap. The Ru_2^{5+} complexes do not axially bind CO while mono- and bis-CO axial adducts are formed for the Ru_2^{4+} and Ru_2^{3+} derivatives, respectively. Six of the eleven investigated compounds exist in a (4,0) isomeric form while five adopt a (3,1) geometric conformation. These two series of compounds thus provide a large enough number of derivatives to examine trends and differences in the spectroscopic data of the two types of isomers in their lower Ru_2^{4+} and Ru_2^{3+} oxidation states. UV–visible spectra of the Ru_2^{4+} derivatives and IR spectra of the Ru_2^{3+} complexes under CO are both isomer dependent, thus suggesting that these data can be used to reliably predict the isomeric form, i.e., (3,1) or (4,0), of diruthenium complexes containing four unsymmetrical substituted anilinopyridinate bridging ligands; this was confirmed by X-ray crystallographic data for seven compounds whose structures were available.

Introduction

Diruthenium complexes bridged by four anionic equatorial ligands containing nitrogen and/or oxygen donor atoms generally exist in a Ru_2^{5+} oxidation state, but a large number of air-stable diruthenium complexes with Ru_2^{4+} or Ru_2^{6+} cores have also been isolated and structurally characterized over the past two decades.[1−15] Most Ru_2^{5+} complexes of this type undergo two metal-centered oxidations and one metal-centered reduction giving compounds with Ru_2^{6+}, Ru_2^{7+}, and Ru_2^{4+} cores, respectively.

A few metal−metal bonded diruthenium complexes in lower valence states, i.e., Ru_2^{3+} and/or Ru_2^{2+}, have also been in-situ electrogenerated from the Ru_2^{5+} and Ru_2^{4+} complexes after axial coordination of the dimetal unit with NO[13,16] or CO.[14] The electrode reactions which lead to these lower diruthenium oxidation states are generally reversible in CH_2Cl_2 and occur with no evidence for cleavage of the metal−metal bond, thus enabling a characterization of the in-situ generated products by thin-layer UV−visible and IR spectroelectrochemistry. However, there is still not sufficient

* Authors to whom correspondence should be addressed. E-mail: kkadish@uh.edu (K.M.K.).
† University of Houston.
‡ Houston Baptist University.

(1) Lindsay, A. J.; Wilkinson, G.; Motevalli, M.; Hursthouse, M. B. *J. Chem. Soc., Dalton Trans.* **1985**, 2321.
(2) Cotton, F. A.; Matusz, M. *J. Am. Chem. Soc.* **1988**, *110*, 5761.
(3) Cotton, F. A.; Miskowski, V. M.; Zhong, B. *J. Am. Chem. Soc.* **1989**, *111*, 6177.
(4) Cotton, F. A.; Ren, T.; Eglin, J. L. *J. Am. Chem. Soc.* **1990**, *112*, 3439.
(5) Cotton, F. A.; Ren, T. *Inorg. Chem.* **1991**, *30*, 3675.
(6) Cotton, F. A.; Walton, R. A. *Multiple Bonds Between Metal Atoms*; Oxford University Press: Oxford, 1993.
(7) Bear, J. L.; Han, B.; Huang, S. *J. Am. Chem. Soc.* **1993**, *115*, 1175−1177.
(8) Cotton, F. A.; Ren, T. *Inorg. Chem.* **1995**, *34*, 3190.
(9) Bear, J. L.; Li, Y.; Han, B.; Van Caemelbecke, E.; Kadish, K. M. *Inorg. Chem.* **1996**, *35*, 3053.
(10) Bear, J. L.; Li, Y.; Han, B.; Kadish, K. M. *Inorg. Chem.* **1996**, *35*, 1395.
(11) Bear, J. L.; Li, Y.; Han, B.; Van Caemelbecke, E.; Kadish, K. M. *Inorg. Chem.* **1997**, *36*, 5449.
(12) Bear, J. L.; Li, Y.; Han, B.; Van Caemelbecke, E.; Kadish, K. M. *Inorg. Chem.* **2001**, *40*, 182.
(13) Bear, J. L.; Wellhoff, J.; Royal, G.; Van Caemelbecke, E.; Eapen, S.; Kadish, K. M. *Inorg. Chem.* **2001**, *40*, 2282.
(14) Kadish, K. M.; Han, B.; Shao, J.; Ou, Z.; Bear, J. L. *Inorg. Chem.* **2001**, *40*, 6848.
(15) Kadish, K. M.; Wang, L.-L.; Thuriere, A.; Van Caemelbecke, E.; Bear, J. L. *Inorg. Chem.* **2003**, *42*, 834.
(16) Lindsay, A. J.; Wilkinson, G.; Motevalli, M.; Hursthouse, M. B. *J. Chem. Soc., Dalton Trans.* **1987**, 2723.

10.1021/ic035026g CCC: $27.50
Published on Web 01/08/2004

Chart 1

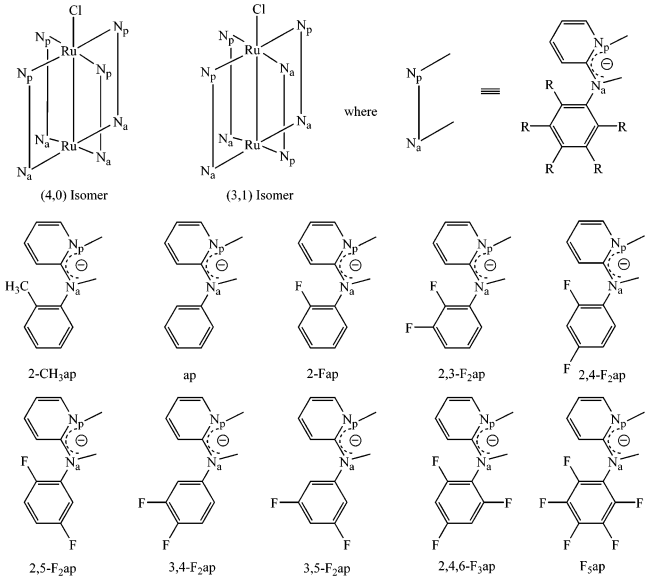

data in the literature to understand relationships between spectral properties (UV−visible or infrared) of the low oxidation state Ru_2^{4+}, Ru_2^{3+}, or Ru_2^{2+} species and electronic properties of the anionic bridging ligands and/or the isomeric form of these compounds which are represented as (4,0), (3,1), (2,2) trans, or (2,2) cis depending upon the substitution pattern of the donor nitrogens with the Ru_2 unit.[11,13,15] This is one goal of the present study which examines the FTIR and UV−visible spectroelectrochemical properties of eleven different Ru_2^{4+} and Ru_2^{3+} derivatives under a CO atmosphere. This data is then used to predict the type of isomer for the starting $Ru_2(L)_4Cl$ complex which was verified by single-crystal X-ray diffraction for seven of the eleven investigated derivatives.

The current work is based on complexes with four identical unsymmetrical substituted anilinopyridine (ap) bridging ligands which exist in a (3,1) or (4,0) isomeric form and builds upon earlier reported electrochemical and spectroscopic results for $Ru_2(dpf)_4(CO)$ which has four identical symmetrical bridging ligands.[14] The first reduction and first oxidation of the dpf complex in CH_2Cl_2, 0.1 M tetra-*n*-butylammonium perchlorate (TBAP) under N_2 leads to stable $[Ru_2(dpf)_4(CO)]^n$ where $n = +1$ or -1. This contrasts with what is observed for the same compound under CO where the resulting products of oxidation and reduction are $[Ru_2(dpf)_4(CO)]^+$, $[Ru_2(dpf)_4(CO)_2]^-$, and $[Ru_2(dpf)_4(CO)_2]^{2-}$, respectively.[14]

The Ru_2^{4+} and Ru_2^{3+} derivatives investigated in the present paper were electrogenerated from substituted anilinopyridine complexes containing a Ru_2^{5+} core and are represented as $Ru_2(L)_4Cl$ where L is one of the anionic bridging ligands in Chart 1. It was anticipated on the basis of our results for $Ru_2(dpf)_4Cl$ and $Ru_2(dpf)_4(CO)$ that the Ru_2^{4+} form of each $Ru_2(L)_4Cl$ derivative might react with CO to yield mono- and/or bis-CO adducts, both of which could then be converted to their Ru_2^{3+} and Ru_2^{2+} forms under the application of a reducing potential. This is indeed the case as shown for four newly synthesized structural isomers of $Ru_2(F_2ap)_4Cl$ (F_2ap = 2,3-F_2ap, 2,4-F_2ap, 3,4-F_2ap, or 3,5-F_2ap) along with seven previously synthesized $Ru_2(L)_4Cl$ complexes (L = 2-CH_3ap, ap, 2-Fap, 2,6-F_2ap, 2,4,6-F_3ap, or F_5ap) which are now examined for the first time as to their electrochemistry, thin-layer FTIR and UV−visible spectroelectrochemistry under a CO atmosphere. Five of the eleven investigated compounds exist in a (4,0) isomeric form while three adopt a (3,1) geometric conformation as verified by single-crystal X-ray diffraction. These two series of compounds thus provide a large enough number of derivatives to examine trends and differences in the spectroscopic data of the two types of isomers in their lower Ru_2^{4+} and Ru_2^{3+} oxidation states in order that predictions as to isomer type may be made for related nonstructurally characterized compounds. As will be shown in the present study, the investigated diruthenium complexes can be divided into two groups on the basis of either their UV−visible spectra in a Ru_2^{4+} oxidation state or the IR spectra of the Ru_2^{3+} complexes under CO. One group corresponds to the (4,0) isomers and the other to the (3,1) isomers.

Experimental Section

Chemicals and Reagents. High-purity nitrogen was purchased from Matheson-Trigas and used as received. High-purity CO gas (purchased from Matheson-Trigas) was bubbled into the solution in order to saturate it with CO prior to measurement. GR graded hexanes, acetones, and absolute dichloromethane (for electrochemistry, UV−visible, and FTIR spectroelectrochemistry) were purchased from Fluka and were used without further purification. Tetra-*n*-butylammonium perchlorate (TBAP), also purchased from Fluka, was twice recrystallized from ethyl alcohol and stored in a vacuum oven at 40 °C for at least one week prior to use. 2-Bromopyridine (C_5H_4NBr), *o*-toluidine ($C_9H_7NH_2$), 2-fluoroaniline ($C_6H_4FNH_2$), 2,3-, 2,4-, 3,5-, 3,4-, and 2,5-difluoroaniline ($C_6H_3F_2NH_2$), 2,4,6-trifluoroaniline ($C_6H_2F_3NH_2$), 2,3,4,5,6-pentafluoroaniline ($C_6F_5NH_2$), 2-anilinopyridine ($C_{11}H_{10}N_2$), lithium chloride (LiCl), ruthenium chloride hydrate ($RuCl_3 \cdot 3H_2O$), silica gel (Merck 230−400 mesh 60 Å), and CD_2Cl_2 (99.8% atom in D, for NMR measurements) were purchased from Aldrich and used as received.

Physical Measurements. Cyclic voltammetry was carried out using either an EG&G Princeton Applied Research (PAR) model 173 or a model 263 potentiostat/galvanostat. A three-electrode system was used and consisted of a glassy carbon working electrode, a platinum wire counter electrode, and a homemade saturated calomel electrode (SCE) as the reference electrode. The SCE was separated from the bulk of the solution by a fritted-glass bridge of low porosity that contained the solvent/supporting electrolyte mixture. All potentials are referenced to the SCE, and all measurements were carried out at room temperature.

Thin-layer time-dependent UV−visible spectral changes were recorded on a Hewlett-Packard model 8453 diode array spectrophotometer using a spectroelectrochemical cell whose design has been reported in the literature.[17] Thin-layer time-dependent infrared spectroelectrochemical measurements were performed using a FTIR Nicolet 550 Magna-IR spectrophotometer with a specially constructed light-transparent FTIR spectroelectrochemical cell.[18] Elemental analyses were carried out by Atlantic microlab, Inc., Norcross, GA. Mass spectra were recorded on a Finnigan TSQ 700

(17) Lin, X. Q.; Kadish, K. M. *Anal. Chem.* **1985**, *57*, 1498.
(18) Lin, X. Q.; Mu, X. H.; Kadish, K. M. *Electroanalysis* **1989**, 35.

instrument at the University of Texas, Austin, or an Applied Biosystem Voyager DE-STR MALDI-TOF mass spectrometer equipped with a nitrogen laser (337 nm) at the University of Houston Mass Spectrometry Laboratory.

Synthesis of Bridging Ligands. All ligands in this work were prepared using a method similar to the one described by Hisano et al.[19] Typically, a mixture of 2-bromopyridine and substituted aniline in a 1:3 molar ratio was heated at 130 °C under N_2 for 10 h. After cooling, the reaction mixture was treated with 10% NaOH aqueous solution (v/v) and steam-distilled. The mixture was then extracted with CH_2Cl_2 and the resulting organic layer dried over $MgSO_4$. After evaporation of solvent, the residue was recrystallized in CH_2Cl_2/hexanes (3/7, v/v) to give a pure white crystalline material.

H(2,3-F_2ap). Yield: 82%. Mass spectral data [*m*/*e*, (fragment)]: 207 $[HF_2ap]^+$, 187 $[HFap]^+$. ^1H NMR (in CD_2Cl_2): 8.26 (d, 1H), 7.97 (m, 1H), 7.57 (t, 1H), 7.08 (m, 1H), 6.34 (t, 4H) ppm (key: d, doublet; t, triplet; m, multiplet).

H(2,4-F_2ap). Yield: 93%. Mass spectral data [*m*/*e*, (fragment)]: 207 $[HF_2ap]^+$, 187 $[HFap]^+$. ^1H NMR (in CD_2Cl_2): 8.21 (s, 1H), 8.07 (m, 1H), 7.54 (d, 1H), 6.93 (t, 2H), 6.81 (d, 1H), 6.72 (d, 2H) ppm (key: d, doublet; t, triplet; m, multiplet).

H(3,4-F_2ap). Yield: 89%. Mass spectral data [*m*/*e*, (fragment)]: 207 $[HF_2ap]^+$, 187 $[HFap]^+$. ^1H NMR (in CD_2Cl_2): 8.23 (d, 1H), 7.61 (m, 2H), 7.15 (m, 2H), 6.81 (m, 2H), 6.63 (bs, 1H) ppm (key: d, doublet; t, triplet; m, multiplet; bs, broad singlet).

H(3,5-F_2ap). Yield: 81%. Mass spectral data [*m*/*e*, (fragment)]: 207 $[HF_2ap]^+$, 187 $[HFap]^+$. ^1H NMR (in CD_2Cl_2): 8.27 (d, 1H), 7.60 (t, 1H), 7.16 (d, 2H), 6.86 (m, 3H), 6.45 (bs, 1H) ppm (key: d, doublet; t, triplet; m, multiplet; bs, broad singlet).

Synthesis of Diruthenium Complexes. (4,0) $Ru_2(2\text{-}CH_3ap)_4Cl$ (**1**), (4,0) $Ru_2(ap)_4Cl$ (**2**), (4,0) $Ru_2(2,5\text{-}F_2ap)_4Cl$ (**4**), (4,0) $Ru_2(F_5ap)_4Cl$ (**6**), (3,1) $Ru_2(2\text{-}Fap)_4Cl$ (**7**), (3,1) $Ru_2(2,4,6\text{-}F_3ap)_4Cl$ (**9**), and (3,1) $Ru_2(F_5ap)_4Cl$ (**11**) were all synthesized as described in the literature.[11,13,15,20] Four different structural isomers of $Ru_2(F_2ap)_4Cl$ were synthesized upon heating a mixture of $Ru_2(O_2CCH_3)_4Cl$ and substituted $H(F_2ap)$ in a 1:20 molar ratio under argon at 120 °C for 8 h. The green solid formed upon cooling the solution to room temperature was dissoved in CH_2Cl_2 and filtered to remove any unreacted $Ru_2(O_2CCH_3)_4Cl$. After evaporation of the solvent, the residue was sublimed under vacuum at 110 °C to remove excess $H(F_2ap)$. The crude product was purified by silica gel column chromatography using a mixture of acetone/*n*-hexane (3:7, v/v) as eluent. Attempts were made to structurally characterize the different $Ru_2(F_2ap)_4Cl$ isomers, but only $Ru_2(3,4\text{-}F_2ap)_4Cl$ (**3**) provided crystals of suitable size for single-crystal X-ray diffraction. The isomeric form of the other three F_2ap derivatives (**5**, **8**, and **10**) is proposed on the basis of the spectral data of the singly and doubly reduced forms of each compound under CO (see later sections of manuscript).

(4,0) $Ru_2(3,4\text{-}F_2ap)_4Cl$ (3). Yield: 63%. Mass spectral data [*m*/*e*, (fragment)]: 1058 $[Ru_2(3,4\text{-}F_2ap)_4Cl]^+$, 1023 $[Ru_2(3,4\text{-}F_2ap)_4]^+$. Anal. Calcd for $C_{44}H_{28}N_8F_8ClRu_2$: C, 49.86; H, 2.64; N, 10.58. Found: C, 50.30; H, 2.85; N, 10.15. UV−vis spectrum in CH_2Cl_2 [λ_{max}, nm ($\epsilon \times 10^{-3}$, M^{-1} cm^{-1}): 422 (5.0), 458 (4.6), 782 (5.5).

(4,0) $Ru_2(3,5\text{-}F_2ap)_4Cl$ (5). Yield: 70%. Mass spectral data [*m*/*e*, (fragment)]: 1058 $[Ru_2(3,5\text{-}F_2ap)_4Cl]^+$, 1023 $[Ru_2(3,5\text{-}F_2ap)_4]^+$. Anal. Calcd for $C_{44}H_{28}N_8F_8ClRu_2$: C, 49.86; H, 2.64; N, 10.58. Found: C, 50.03; H, 2.70; N, 10.29. UV−vis spectrum in CH_2Cl_2 [λ_{max}, nm ($\epsilon \times 10^{-3}$, M^{-1} cm^{-1}): 417 (4.8), 464 (4.4), 794 (5.5).

Table 1. Crystal Data and Data Collection and Processing Parameters for (4,0) $Ru_2(3,4\text{-}F_2ap)_4Cl$ (**3**)

space group	*P*4/*n* tetragonal
cell constant	
a (Å)	15.5421 (10)
b (Å)	15.5421 (10)
c (Å)	9.8885 (9)
α (deg)	90.00
β (deg)	90.00
γ (deg)	90.00
V (Å^3)	2388.6 (3)
mol formula	$C_{44}H_{28}N_8F_8ClRu_2 \cdot C_6H_{14}$
fw (g/mol)	1144.51
Z	2
ρ_{calcd} (g/cm^3)	1.591
μ (cm^{-1})	0.764
λ (Mo Kα) (Å)	0.71073
temp (K)	223
R (F_o)[a]	0.0339
R_w (F_o)[b]	0.0897

[a] $R = \sum||F_o| - |F_c||/\sum|F_o|$. [b] $R_w = [\sum_w(|F_o| - |F_c|)^2/\sum_w|F_o|^2]^{1/2}$.

(3,1) $Ru_2(2,4\text{-}F_2ap)_4Cl$ (8). Yield: 63%. Mass spectral data [*m*/*e*, (fragment)]: 1058 $[Ru_2(2,4\text{-}F_2ap)_4Cl]^+$, 1023 $[Ru_2(2,4\text{-}F_2ap)_4]^+$. Anal. Calcd for $C_{44}H_{28}N_8F_8ClRu_2$: C, 49.86; H, 2.64; N, 10.58. Found: C, 50.28; H, 2.80; N, 10.28. UV−vis spectrum in CH_2Cl_2 [λ_{max}, nm ($\epsilon \times 10^{-3}$, M^{-1} cm^{-1}): 423 (6.2), 471 (5.9), 760 (6.3).

(3,1) $Ru_2(2,3\text{-}F_2ap)_4Cl$ (10). Yield: 60%. Mass spectral data [*m*/*e*, (fragment)]: 1058 $[Ru_2(2,3\text{-}F_2ap)_4Cl]^+$, 1023 $[Ru_2(2,3\text{-}F_2ap)_4]^+$. Anal. Calcd for $C_{44}H_{28}N_8F_8ClRu_2$: C, 49.86; H, 2.64; N, 10.58. Found: C, 50.12; H, 2.78; N, 10.21. UV−vis spectrum in CH_2Cl_2 [λ_{max}, nm ($\epsilon \times 10^{-3}$, M^{-1} cm^{-1}): 420 (4.2), 466 (4.2), 760 (4.4).

X-ray Crystallography of (4,0) $Ru_2(3,4\text{-}F_2ap)_4Cl$ (3). A single-crystal X-ray crystallographic study was performed at the University of Houston X-ray Crystallographic Center. A dark green crystal was placed in a stream of dry nitrogen gas at −50 °C in a random position. The radiation used was Mo Kα monochromatized by a highly ordered graphite crystal. Final cell constants as well as other information pertinent to data collection and structure refinement are listed in Table 1.

All measurements were made with a Siemens SMART platform diffractometer equipped with a 1K CCD area detector. A hemisphere of data 1271 frames at 5 cm detector distance was collected using a narrow-frame method with scan widths of 0.30° in ω and an exposure time of 30 s/frame. The first 50 frames were remeasured at the end of data collection to monitor instrument and crystal stability and the maximum correction on I was <1%. The data were integrated using the Siemens SAINT program, with the intensities corrected for Lorentz factor, polarization, air absorption, and absorption due to variation in the path length through the detector faceplate. A ψ-scan absorption correction was applied based on the entire data set. Redundant reflections were averaged. Final cell constants were refined using 5000 reflections having $I > 10\sigma(I)$. The Laue symmetry was determined to be 4/*m*, and from the systematic absences noted the space group was shown unambiguously to be *P*4/*n*. The Ru_2 molecule was found to be disordered although it is not clear whether this is a true disorder or simply a case of minor twinning. For any given line of molecules along the unique *c* axis, the crystallographic average shows 80% of the molecules to have one torsional N−Ru−Ru−N handedness, while the other 20% have the opposite. The two different conformations are displaced slightly along the *c* axis such that the axial chloride of one lies at essentially the same location as the Ru_2 atom of the other. Since *P*4/*n* is a centrosymmetric space group, every other line of molecules is the reverse of this. For convenience, the 20%

(19) Hisano, T.; Matsuoka, T.; Tsutsumi, K.; Muraoka, K.; Ichikawa, M. *Chem. Pharm. Bull.* **1981**, *29*, 3706.
(20) Chakravarty, A. R.; Cotton, F. A.; Tocher, D. A. *Inorg. Chem.* **1985**, *24*, 172.

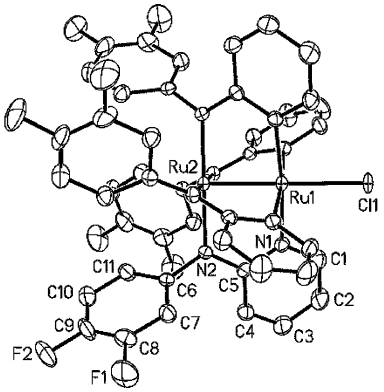

Figure 1. Molecular structure of (4,0) $Ru_2(3,4\text{-}F_2ap)_4Cl$ (**3**). H atoms have been omitted for clarity.

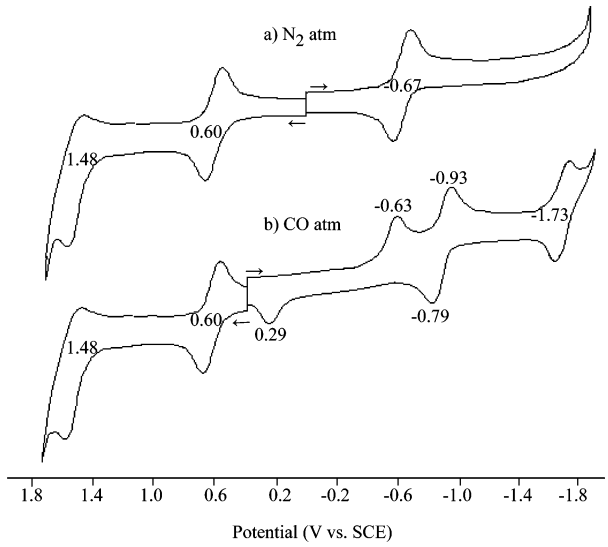

Figure 2. Cyclic voltammograms of (4,0) $Ru_2(3,4\text{-}F_2ap)_4Cl$ (**3**) in CH_2Cl_2, 0.1 M TBAP (a) under N_2 and (b) under a CO atmosphere. Scan rate = 0.1 V/s.

minor component was modeled as a rigid body having the opposite torsional twist of the 80% major component and situated as if they are mirrored through the pyridine ring. It is sterically impossible for the two different models to coexist in the same line along *c*, but it is not clear whether the individual lines of molecules in the crystal are randomly disposed (disorder) or if there are two separate uniform zones (twinning). The ORTEP diagram of $Ru_2(3,4\text{-}F_2ap)_4Cl$ is illustrated in Figure 1, and there is no ambiguity that the compound exists in a (4,0) isomeric form. All intramolecular bond lengths and angles as well as other structural data of this compound is given in the Supporting Information.

Results and Discussion

Electrochemistry. Figure 2 illustrates cyclic voltammograms of (4,0) $Ru_2(3,4\text{-}F_2ap)_4Cl$ in CH_2Cl_2 containing 0.1 M TBAP under both N_2 and CO atmospheres. The other investigated Ru_2^{5+} complexes exhibit similar shaped cyclic voltammograms with values of $E_{1/2}$ for each electrode reaction depending upon the specific number and position of substituents of the ap ligand. The half-wave or peak potentials for the $Ru_2^{5+/4+}$, $Ru_2^{4+/3+}$, and $Ru_2^{3+/2+}$ processes of $Ru_2(L)_4Cl$ (L is one of the anionic ligands shown in Chart 1) are summarized in Table 2 under an N_2 or CO atmosphere. $E_{1/2}$ values for oxidation of these compounds ($Ru_2^{5+/6+}$ and $Ru_2^{6+/7+}$) are the same under N_2 or CO, consistent with a lack of CO binding to the neutral and/or Ru_2^{6+} and Ru_2^{7+} oxidation states. A summary of these oxidation potentials is given in Table S1 (Supporting Information).

Each $Ru_2(L)_4Cl$ complex undergoes a single reversible one-electron reduction in CH_2Cl_2, 0.1 M TBAP under N_2, but three one-electron reductions are seen in the same solvent/supporting electrolyte mixture under a CO atmosphere (Figure 2b and Table 2). The first reduction of all eleven compounds is irreversible under CO, and the cathodic peak potential, E_{pc}, is coupled with a reoxidation peak whose E_{pa} value ranges from 0.13 to 0.58 V for the (4,0) isomers and from 0.12 to 0.47 V for the (3,1) isomers (see Table 2). The second reduction under CO is also not reversible as indicated by the larger than 60 mV potential separation between E_{pc} and E_{pa} (100−230 mV) while the third reduction of all eleven compounds is reversible.

The reduction of $Ru_2(dpf)_4Cl$ under CO leads to $Ru_2(dpf)_4(CO)$, which was structurally characterized,[14] and this Ru_2^{4+} complex is converted to its Ru_2^{3+} and Ru_2^{2+} forms in two reversible one-electron transfer steps. The $Ru_2^{4+/3+}$ process of $Ru_2(dpf)_4(CO)$ under CO is also accompanied by axial coordination of a second CO molecule, thus giving a $Ru_2(dpf)_4(CO)/[Ru_2(dpf)_4(CO)_2]^-$ couple under CO which is shifted positively by 100 mV from the $E_{1/2}$ value obtained for the $Ru_2^{4+/3+}$ process assigned to $Ru_2(dpf)_4(CO)^{0/-1}$ under a N_2 atmosphere.

The existence of two additional reduction processes after formation of Ru_2^{4+} for the eleven investigated $Ru_2(L)_4Cl$ complexes under CO (see Table 2) and the irreversible character of the $Ru_2^{5+/4+}$ process (see Figure 2b for the case of (4,0) $Ru_2(3,4\text{-}F_2ap)_4Cl$ (**3**)) suggest a similar mechanism for all of the $Ru_2(L)_4Cl$ derivatives as was reported for $Ru_2(dpf)_4Cl$ which is electroreduced to give $Ru_2(dpf)_4(CO)$.[14] The second and third reductions of $Ru_2(L)_4Cl$ under CO are thus assigned to the $Ru_2^{4+/3+}$ and $Ru_2^{3+/2+}$ redox couples as indicated in Table 2.

The dependence of $E_{1/2}$ on the electronic effect of the ap substituents can be quantified by linear least-squares fit of the data to the Hammett relationship shown in eq 1:[21,22]

$$\Delta E_{1/2} = 4\sum\sigma\rho \qquad (1)$$

where ρ is the reactivity constant and $4\sum\sigma$ is the overall electronic effect of the four bridging ligands. Plots of $E_{1/2}$ (or E_{pc}) vs the sum of substituent constants ($4\sum\sigma$)[23] (eq 1) are shown in Figure 3a for the (4,0) isomers and Figure 3b for the (3,1) isomers under (i) N_2 and (ii) CO atmospheres. A linear relationship is observed in all cases, thus suggesting a similar electron transfer mechanism throughout the series of compounds for each redox couple, i.e., $Ru_2^{5+/4+}$, $Ru_2^{4+/3+}$, and $Ru_2^{3+/2+}$. The ρ value under CO ranges between 54 and 84 mV with the exact value depending upon both the nature

(21) Zuman, P. *The Elucidation of Organic Electrode Process*; Academic Press: London, 1967.
(22) Hammett, L. P. *Physical Organic Chemistry*; Wiley: New York, 1970.
(23) Zuman, P. *Substituent Effects in Organic Polarography*; Plenum Press: New York, 1967.

Table 2. Half-Wave Potentials (V vs SCE) for Electroreduction of the (4,0) and (3,1) Isomers of $Ru_2(L)_4Cl$ in CH_2Cl_2 Containing 0.1 M TBAP under a N_2 or CO Atmosphere

			under N_2	under CO						
				$Ru_2^{5+/4+}$			$Ru_2^{4+/3+}$			$Ru_2^{3+/2+}$
isomer type	ligand, $\sum\sigma$	ligand, L	$E_{1/2}$	E_{pc}	E_{pa}	ΔE^a	E_{pc}	E_{pa}	ΔE^a	$E_{1/2}$
(4,0)	−0.17	2-CH_3ap (**1**)	−0.89	−0.80	0.13	0.93	−1.12	−1.02	0.10	−1.96
	0.00	ap (**2**)	−0.86	−0.78	0.17	0.95	−1.08	−0.94	0.14	−1.88
	+0.40	3,4-F_2ap (**3**)	−0.67	−0.63	0.29	0.92	−0.93	−0.79	0.14	−1.73
	+0.58	2,5-F_2ap (**4**)	−0.63	−0.60	0.39	0.99	−0.91	−0.76	0.15	−1.68
	+0.68	3,5-F_2ap (**5**)	−0.58	−0.54	0.42	0.96	−0.86	−0.74	0.12	−1.65
	+1.22	F_5ap (**6**)	−0.35	−0.42	0.58	1.00	−0.75	−0.57	0.18	−1.56
(3,1)	+0.24	2-Fap (**7**)	−0.77	−0.73	0.12	0.85	−1.04	−0.83	0.21	−1.73
	+0.30	2,4-F_2ap (**8**)	−0.70	−0.69	0.18	0.87	−1.00	−0.77	0.23	−1.72
	+0.54	F_3ap (**9**)	−0.65	−0.58	0.23	0.81	−0.88	−0.75	0.13	−1.69
	+0.58	2,3-F_2ap (**10**)	−0.62	−0.60	0.26	0.86	−0.93	−0.73	0.20	−1.67
	+1.22	F_5ap (**11**)	−0.35	−0.39	0.47	0.86	−0.77	−0.57	0.20	−1.52

[a] $\Delta E = |E_{pc} - E_{pa}|$ in V.

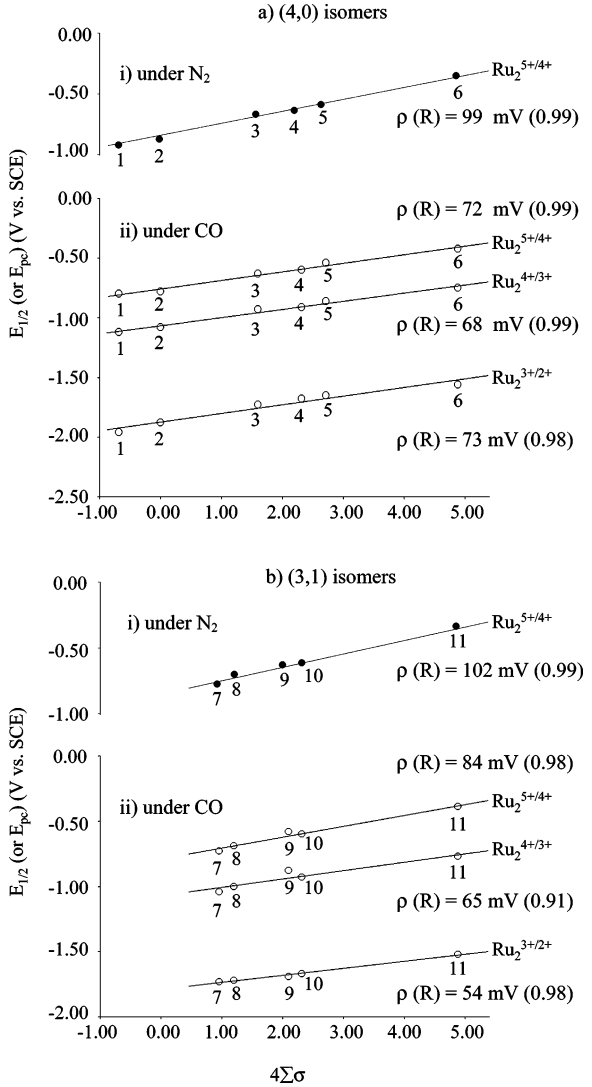

Figure 3. Linear free energy relationships for reduction of (a) (4,0) isomers and (b) (3,1) isomers of $Ru_2(L)_4Cl$ under (i) N_2 and (ii) CO atmospheres

of the redox reaction and the type of geometric isomer. The ρ value of the $Ru_2^{5+/4+}$ process under CO is smaller in magnitude than the ρ value of $Ru_2^{5+/4+}$ under N_2 for each series of isomers, and this may be accounted for by a shift of electron density from the Ru_2 core to the axial CO ligand

Table 3. UV−Vis Spectral Data for Neutral, Singly and Doubly Reduced (4,0) and (3,1) Isomers of $Ru_2(L)_4Cl$ in CH_2Cl_2 Containing 0.2 M TBAP under a CO Atmosphere

			λ_{max}, nm ($\epsilon \times 10^{-3}$, M^{-1} cm^{-1})			ϵ_{II}/ϵ_I
isomer type	oxidation state	ligand, L	band I	band II	band III	(Ru_2^{4+})
(4,0)	Ru_2^{5+}	2-CH_3ap (**1**)	424 (4.3)	461 (4.7)	764 (7.3)	
		ap (**2**)	421 (5.8)	452 (5.7)	778 (7.0)	
		3,4-F_2ap (**3**)	422 (4.2)	458 (4.6)	782 (5.5)	
		2,5-F_2ap (**4**)	422 (4.8)	466 (5.3)	774 (5.8)	
		3,5-F_2ap (**5**)	417 (4.8)	464 (4.4)	794 (5.5)	
		F_5ap (**6**)	414 (4.8)	483 (5.9)	903 (4.7)	
	Ru_2^{4+}	2-CH_3ap (**1**)	464 (7.3)	646 (7.9)		1.08
		ap (**2**)	459 (6.8)	631 (7.1)		1.04
		3,4-F_2ap (**3**)	461 (5.4)	635 (5.5)		1.01
		2,5-F_2ap (**4**)	466 (5.5)	619 (5.7)		1.04
		3,5-F_2ap (**5**)	462 (5.4)	633 (5.8)		1.07
		F_5ap (**6**)	478 (4.9)	595 (5.4)		1.10
	Ru_2^{3+}	2-CH_3ap (**1**)	480 (sh)			
		ap (**2**)	485 (sh)			
		3,4-F_2ap (**3**)	525 (sh)			
		2,5-F_2ap (**4**)	470 (sh)			
		3,5-F_2ap (**5**)	460 (sh)			
		F_5ap (**6**)	459 (sh)			
(3,1)	Ru_2^{5+}	2-Fap (**7**)	428 (3.6)	463 (3.6)	750 (3.9)	
		2,4-F_2ap (**8**)	420 (4.0)	466 (3.8)	761 (4.1)	
		2,4,6-F_3ap (**9**)	418 (4.5)	476 (4.7)	777 (4.5)	
		2,3-F_2ap (**10**)	422 (4.2)	468 (4.2)	759 (4.4)	
		F_5ap (**11**)	414 (3.1)	486 (3.0)	791 (2.8)	
	Ru_2^{4+}	2-Fap (**7**)	468 (5.0)	579 (6.2)	903 (1.6)	1.24
		2,4-F_2ap (**8**)	472 (6.1)	560 (8.5)	912 (1.5)	1.39
		2,4,6-F_3ap (**9**)	474 (7.0)	551 (10.1)	918 (1.8)	1.44
		2,3-F_2ap (**10**)	473 (6.9)	581 (8.8)	916 (1.4)	1.28
		F_5ap (**11**)	480 (3.1)	568 (3.8)	957 (1.1)	1.23
	Ru_2^{3+}	2-Fap (**7**)	422 (11.0)	468 (sh)		
		2,4-F_2ap (**8**)	480 (sh)			
		2,4,6-F_3ap (**9**)	419 (15.3)	474 (sh)		
		2,3-F_2ap (**10**)	473 (sh)			
		F_5ap (**11**)	475 (sh)			

due to its π back-bonding ability, thus diminishing the influence of the substituents on the bridging ligands.

UV−Visible Spectroelectrochemistry. UV−visible data for the investigated $Ru_2(L)_4Cl$ complexes under CO in their neutral (Ru_2^{5+}), singly reduced (Ru_2^{4+}), and doubly reduced (Ru_2^{3+}) forms are summarized in Table 3. Spectra in the lower two oxidation states were obtained by thin-layer spectroelectrochemistry with examples of the time-dependent UV−visible spectral changes that occur during the $Ru_2^{5+/4+}$

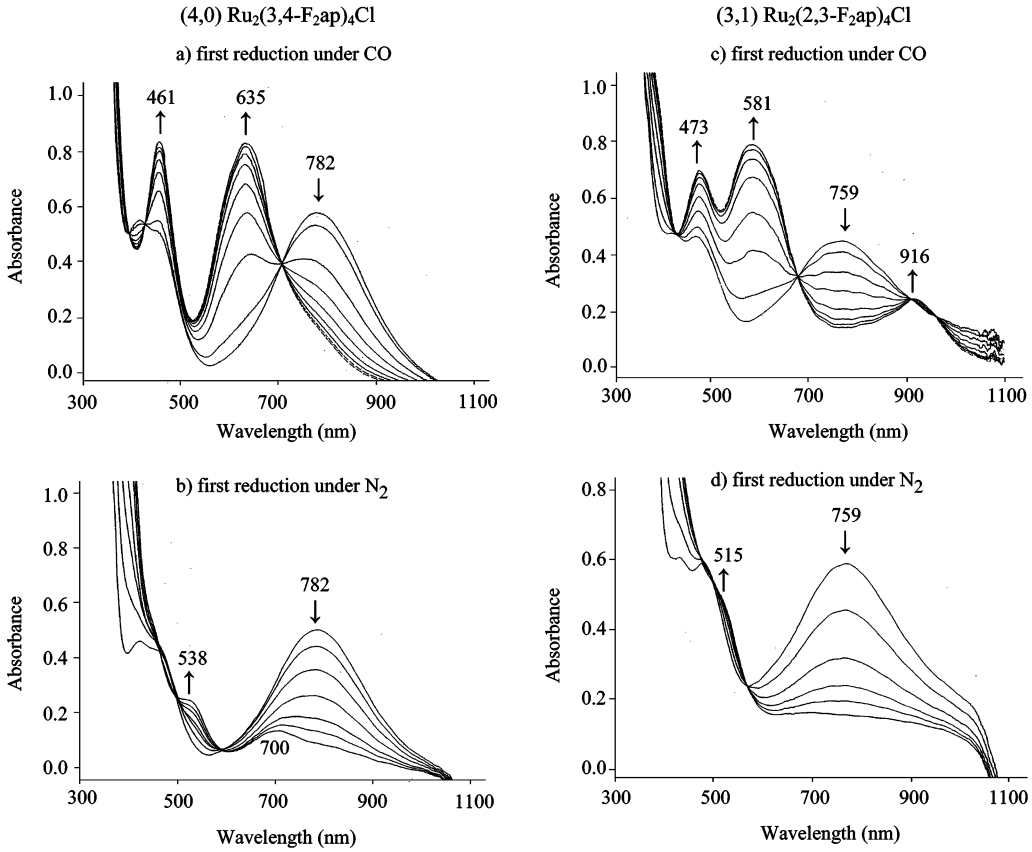

Figure 4. Time-dependent UV−visible spectral changes for first reduction of (4,0) $Ru_2(3,4\text{-}F_2ap)_4Cl$ (**3**) in CH_2Cl_2, 0.2 M TBAP (a) under CO and (b) under N_2 and for first reduction of (3,1) $Ru_2(2,3\text{-}F_2ap)_4Cl$ (**10**) in CH_2Cl_2, 0.2 M TBAP (c) under CO and (d) under N_2.

process illustrated in Figures 4a and 4c for the case of (4,0) $Ru_2(3,4\text{-}F_2ap)_4Cl$ and (3,1) $Ru_2(2,3\text{-}F_2ap)_4Cl$, respectively. This figure also includes, for comparison purposes, the time-dependent UV−visible spectral changes seen for the same $Ru_2^{5+/4+}$ electrode reactions in CH_2Cl_2, 0.2 M TBAP under N_2 (Figures 4b and 4d).

The UV−visible spectrum of neutral $Ru_2(3,4\text{-}F_2ap)_4Cl$ is the same under N_2 and CO (as expected because there is no CO binding to Ru_2^{5+}), but significant spectral differences exist between the electrogenerated Ru_2^{4+} species under these two experimental conditions. In both cases, the major absorption band of $Ru_2(3,4\text{-}F_2ap)_4Cl$ at 782 nm in CH_2Cl_2, 0.2 M TBAP decreases in intensity as the reduction proceeds, and this leads either to a spectrum with two intense bands at 461 and 635 nm under CO (Figure 4a) or to one with two weak absorption bands at 538 and 700 nm for the same solution under N_2 (Figure 4b). Similar types of spectral changes (as shown in Figures 4a and 4b) occur upon reduction of compounds **1**, **2**, **4**, **5**, and **6** under CO or N_2, and the data under CO is summarized in Table 3, which lists the values of λ_{max} and ϵ for each singly and doubly reduced complex.

The above results on Ru_2^{4+} for compounds **1**−**6** contrast with what is observed in the case of compounds **7**−**11** where the electrogenerated Ru_2^{4+} complex under CO has three rather than two absorption bands, one at 468−480 nm, one at 551−581 nm, and one at 903−957 nm (see Table 3). An example of the spectral changes which occur upon the first one-electron reduction of these four complexes is shown in Figures 4c and 4d for (3,1) $Ru_2(2,3\text{-}F_2ap)_4Cl$ (**10**) under CO and under N_2, respectively.

Another difference between the Ru_2^{4+} spectra for compounds **1**−**6** and those for compounds **7**−**11** is the ratio of molar absorptivities between the bands labeled as I and II in Table 3. Complexes **1**−**6** have an ϵ_{II}/ϵ_I ratio of 1.01−1.10 while compounds **7**−**11** have a higher ϵ_{II}/ϵ_I ratio of 1.23 to 1.44 (see Table 3). This difference between the number and relative intensity of the absorption bands in the two types of Ru_2^{4+} spectra is attributed to differences in the isomer type of the compounds which were structurally characterized in their Ru_2^{5+} form as (4,0) in the case of **1**−**4** and (3,1) in the case of **7** and **9**. $Ru_2(3,5\text{-}F_2ap)_4Cl$ (**5**) and **6** are the only derivatives with a two-banded Ru_2^{4+} spectra and an ϵ_{II}/ϵ_I ratio of ≈1.0 which was not structurally characterized, and this compound is now assigned as a (4,0) isomer on the basis of its spectral similarity to compounds **1**−**4** in the Ru_2^{4+} oxidation state under CO. Also, $Ru_2(2,4\text{-}F_2ap)_4Cl$ (**8**) and $Ru_2(2,3\text{-}F_2ap)_4Cl$ (**10**) are the only two derivatives with a three-banded Ru_2^{4+} spectrum under CO and an ϵ_{II}/ϵ_I ratio which is significantly greater than 1.0 which have not been structurally characterized, and these two compounds are now assigned as (3,1) isomers on the basis of their spectral similarities to compounds **7** and **9** in their Ru_2^{4+} oxidation state under CO. It should be noted that **6** and **11** were only indirectly characterized as (4,0) and (3,1) isomers and both of them also follow the trend of other (3,1) and (4,0) isomers in Table 3.

Table 4. CO Stretching Frequencies (ν_{CO}, cm^{-1}) for Ru_2^{n+} Forms of $Ru_2(L)_4Cl$ in CH_2Cl_2 Containing 0.2 M TBAP

isomer type	ligand, $\sum\sigma^a$	ligand, L	Ru_2^{4+}	Ru_2^{3+} weak	Ru_2^{3+} strong	Ru_2^{2+}
(4,0)	−0.17	2-CH_3ap (**1**)	1872	1872	1798	
	0.00	ap (**2**)	1876	1876	1805	
	+0.40	3,4-F_2ap (**3**)	1887	1887	1815	
	+0.58	2,5-F_2ap (**4**)	1891	1891	1819	
	+0.68	3,5-F_2ap (**5**)	1893	1893	1820	
	+1.22	F_5ap (**6**)	1911	1911	1828	1757
(3,1)	+0.24	2-Fap (**7**)	1883	1870	1818	
	+0.30	2,4-F_2ap (**8**)	1885	1874	1820	
	+0.54	2,4,6-F_3ap (**9**)	1888	1876	1822	1745
	+0.58	2,3-F_2ap (**10**)	1891	1878	1825	
	+1.22	F_5ap (**11**)	1900	1885	1834	1757

[a] Taken from ref 22.

Additional diagnostic criteria (and identical conclusions) as to the isomer type can be formulated on the basis of the IR data for the Ru_2^{3+} derivatives under CO (see section below), but the UV−visible data alone is self-consistent and clearly suggests that the UV−visible spectrum of the Ru_2^{4+} complex under CO can be used as a simple diagnostic criterion to determine the exact isomer type of the initial Ru_2^{5+} species in the absence of structural data.

Infrared Spectroelectrochemistry. The cyclic voltammetric data described earlier in the manuscript is consistent with the overall mechanism shown by eqs 2−4.

$$Ru_2(L)_4Cl + e^- + CO \rightleftarrows Ru_2(L)_4(CO) + Cl^- \quad (2)$$

$$Ru_2(L)_4(CO) + e^- + CO \rightleftarrows [Ru_2(L)_4(CO)_2]^- \quad (3)$$

$$[Ru_2(L)_4(CO)_2]^- + e^- \rightleftarrows [Ru_2(L)_4(CO)_2]^{2-} \quad (4)$$

Thin-layer IR spectroelectrochemistry was used to measure the CO stretching frequencies for the electrogenerated Ru_2^{4+}, Ru_2^{3+}, and in part Ru_2^{2+} species in CH_2Cl_2, 0.2 M TBAP under a CO atmosphere. Earlier spectroelectrochemical studies[14] on $[Ru_2(dpf)_4(CO)]^n$ where $n = 1$, 0, or −1 showed a shift in ν_{CO} from 2019 cm^{-1} for $n = +1$ (Ru_2^{5+}) to 1929 cm^{-1} for $n = 0$ (Ru_2^{4+}) to 1842 cm^{-1} for $n = -1$ (Ru_2^{3+}), and it was of interest to see if a similar shift of 87−89 cm^{-1} per unit change of oxidation state might also be observed for the currently investigated anilinopyridinate complexes which differ from the dpf derivative both in symmetry (the dpf ligand is symmetrical and the substituted ap ligands in Chart 1 are not) and in basicity of the bridging ligand (ap is more basic than dpf).

Results of the IR spectroelectrochemical studies are summarized in Table 4, which lists ν_{CO} values of the electrogenerated Ru_2^{4+}, Ru_2^{3+}, and Ru_2^{2+} species, while examples of the thin-layer difference spectra are illustrated in Figure 5 for the Ru_2^{4+} and Ru_2^{3+} forms of (4,0) Ru_2(3,4-F_2ap)$_4$Cl (**3**) and (3,1) Ru_2(2,3-F_2ap)$_4$Cl (**10**) in CH_2Cl_2, 0.2 M TBAP under CO. The infrared spectra of the Ru_2^{4+} and Ru_2^{3+} species were examined for all eleven compounds in the region of ν_{CO} while those of the Ru_2^{2+} products were limited only to the (4,0) and (3,1) isomers of $Ru_2(F_5ap)_4Cl$ (**6** and **11**) and (3,1) Ru_2(2,4,6-F_3ap)$_4$Cl (**9**).

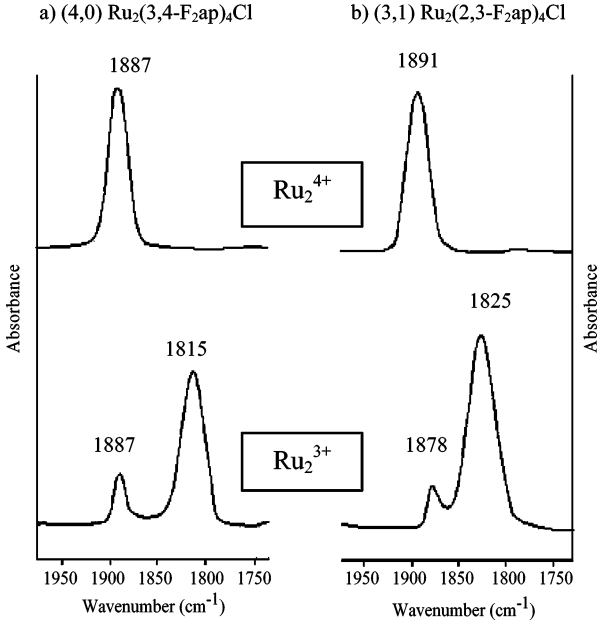

Figure 5. Thin-layer FTIR spectra for electrogenerated Ru_2^{4+} and Ru_2^{3+} forms of (a) (4,0) Ru_2(3,4-F_2ap)$_4$Cl (**3**) and (b) (3,1) Ru_2(2,3-F_2ap)$_4$Cl (**10**) in CH_2Cl_2, 0.2 M TBAP.

None of the neutral Ru_2^{5+} species binds CO while the one-electron reduction product shows a single well-defined ν_{CO} stretch which ranges from 1872 to 1911 cm^{-1} for compounds **1**−**6** which are assigned as (4,0) isomers on the basis of UV−visible and structural data. Similar ν_{CO} values of 1883 to 1900 cm^{-1} are seen for compounds **7**−**11** which, in this case, are assigned as being (3,1) isomers. Only a single CO band is seen after the first one-electron reduction of each $Ru_2(L)_4Cl$ complex under CO, thus suggesting that one and only one CO molecule is axially coordinated to the dimetal unit of the eleven Ru_2^{4+} compounds, a result consistent with the previous crystal structure of $Ru_2(dpf)_4CO$.[14] Unfortunately, crystal structures of the currently investigated Ru_2^{4+} species under CO could not be obtained to confirm this assignment and thus determine the exact formulation of the electrogenerated CO adduct.

The Ru_2^{3+} species obtained after the one-electron reduction of $Ru_2(L)_4(CO)$ are characterized by two IR bands of different intensities (see Figure 5). This suggests the presence of two interacting CO molecules and is consistent with the cyclic voltammetric data under CO which suggests that two CO molecules are axially coordinated to the dimetal unit of the electrogenerated Ru_2^{3+} complex. This is also what was seen in the case of the dpf complex in its Ru_2^{3+} oxidation state. The most intense IR bands of the Ru_2^{3+} complexes in the present study are 71−83 cm^{-1} lower than the ν_{CO} stretch of the six (4,0) $Ru_2(L)_4(CO)$ complexes and 65−66 cm^{-1} lower than the ν_{CO} stretch for the five (3,1) $Ru_2(L)_4(CO)$ derivatives (see Table 4). Thus, these shifts in ν_{CO} upon going from Ru_2^{4+} to Ru_2^{3+} are slightly less than the 87−89 cm^{-1} shifts in the CO stretching vibrations upon going from $Ru_2(dpf)_4(CO)$ to $[Ru_2(dpf)_4(CO)]^-$ or $[Ru_2(dpf)_4(CO)_2]^-$ in CH_2Cl_2, 0.2 M TBAP.[14]

The weakest band in the infrared spectra of each electrogenerated Ru_2^{3+} complex is located at exactly the same ν_{CO}

Table 5. Isomer Type Based on X-ray Structures of Ru_2^{5+}, UV−Vis Data of Ru_2^{4+}, and IR Data of Ru_2^{3+} for $Ru_2(L)_4Cl$ Complexes under a CO Atmosphere

isomer type	ligand	compd no.	X-ray structures of Ru_2^{5+}	UV−vis of Ru_2^{4+} ϵ_{II}/ϵ_I	IR of Ru_2^{3+} $\Delta\nu_{CO}$ $\lvert Ru_2^{4+} - Ru_2^{3+}\rvert$
(4,0)	2-CH_3ap	**1**	(4,0)	1.08	0
	ap	**2**	(4,0)	1.04	0
	3,4-F_2ap	**3**	(4,0)	1.01	0
	2,5-F_2ap	**4**	(4,0)	1.04	0
	3,5-F_2ap	**5**		1.07	0
	F_5ap[a]	**6**	(4,0)		0
(3,1)	2-Fap	**7**	(3,1)	1.24	13
	2,4-F_2ap	**8**		1.39	11
	2,4,6-F_3ap	**9**	(3,1)	1.44	12
	2,3-F_2ap	**10**		1.28	13
	F_5ap[a]	**11**	(3,1)		15

[a] Crystal structures for the (4,0) and (3,1) isomers of $Ru_2(F_5ap)_4(C{\equiv}CC_6H_5)_2$ were already reported and are the basis for assigning the isomer type in compounds **6** and **11**, respectively. See ref 11.

as the single CO band for the (4,0) isomers of $Ru_2(L)_4(CO)$, but it is at 11−15 cm^{-1} lower than the single CO band of the (3,1) isomers of $Ru_2(L)_4(CO)$ having the same bridging ligands. Thus, this difference in IR spectra between the two series of compounds (**1**−**6** and **7**−**11**) might also be used as an additional spectroscopic criterion to distinguish between (3,1) and (4,0) isomers when no crystal structure of the Ru_2^{5+} complex is available.

The UV−visible and IR spectroscopic data are self-consistent and agree with the isomer type determined by X-ray crystallography. These results are summarized in Table 5.

As shown in Table 4, the ν_{CO} values for the Ru_2^{n+} ($n = 3$ or 4) forms of the compounds increase as the electron-withdrawing ability of the substituent on the bridging ligand increases, thus suggesting that the C≡O bond is stronger in compounds which have less basic bridging ligands (i.e., F_5ap). The electrogenerated CO adducts of Ru_2^{4+} and Ru_2^{3+} both exhibit linear free energy relationships between ν_{CO} and $4\sum\sigma$.[23] This is shown in Figure 6a for the case of the (4,0) isomers and Figure 6b for the case of the (3,1) isomers. The data can then be fitted with the Hammett relationship expressed by eq 5[21,22] with ρ values ranging from 4.0 to 6.9 cm^{-1}.

$$\Delta\nu = 4\Sigma\sigma\rho \qquad (5)$$

The effect of the substituent's electronic properties on ν_{CO} was previously measured for a series of Rh_2^{4+} complexes containing four substituted formamidinate bridging ligands and one CO molecule axially coordinated to the dimetal unit. The study revealed that ν_{CO} increases linearly as the electron-withdrawing effect of the substituent on the bridging ligand increases, and this was accounted for by a decreased π-back-bonding effect between the metal ($d\pi$) and the $2p\pi^*$ of CO, owing to a decrease in the electron density on the dimetal unit.[24] A similar explanation can be proposed to rationalize the data in Figures 6a and 6b.

(24) Ren, T. *Coord. Chem. Rev.* **1998**, *175*, 43.

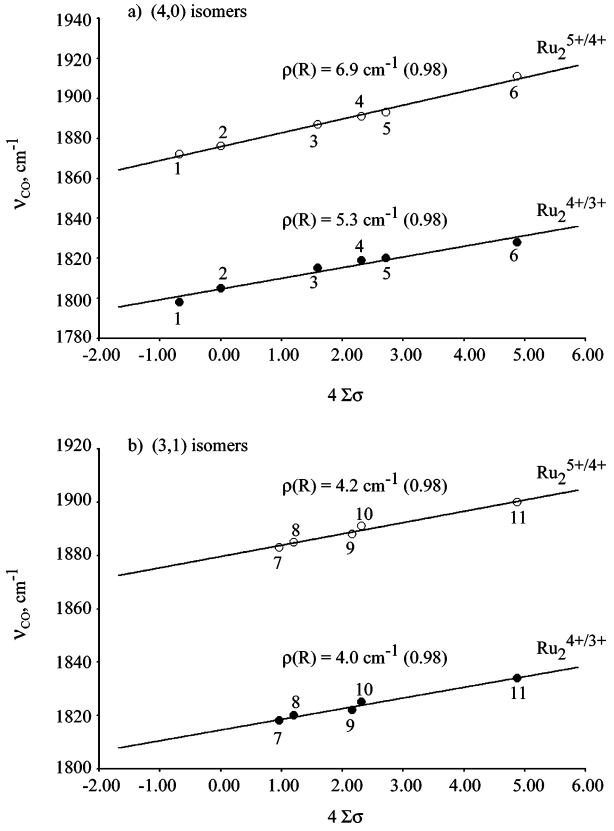

Figure 6. Linear free energy relationships between ν_{CO} and $4\sum\sigma$ for (a) (4,0) isomers and (b) (3,1) isomers of the 11 investigated compounds.

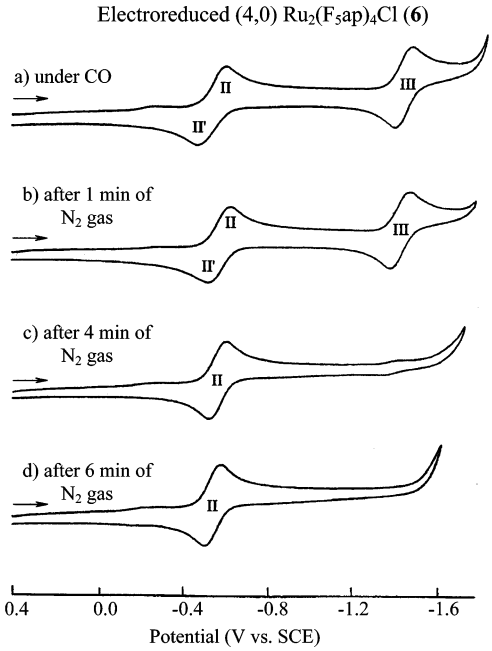

Figure 7. Cyclic voltammograms of electroreduced (4,0) $Ru_2(F_5ap)_4Cl$ (**6**) under (a) CO and (b−d) N_2 gas in CH_2Cl_2, 0.1 M TBAP. Scan rate = 0.1 V/s.

Stability of (4,0) $[Ru_2(F_5ap)_4(CO)_x]^n$ ($x = 1$ or 2 and $n = 0$ or −1). The (4,0) isomer of $Ru_2(F_5ap)_4(CO)$ was in-situ electrogenerated by controlled-potential electrolysis of (4,0) $Ru_2(F_5ap)_4Cl$ in CH_2Cl_2, 0.2 M TBAP under CO (P_{CO} = 0.44 atm) at −0.50 V. As shown in Figure 7a, the electrogenerated product undergoes two well-defined one-

electron reductions under CO (labeled as II and III) whose potentials match exactly those for the second and third reductions of (4,0) $Ru_2(F_5ap)_4Cl$ in CH_2Cl_2, 0.1 M TBAP under CO (see Table 2), thus confirming the formation of a stable (4,0) $Ru_2(F_5ap)_4(CO)$ complex after bulk electrolysis.

To evaluate the stability of the CO adduct on the further reduced forms of (4,0) $Ru_2(F_5ap)_4(CO)$ and to determine whether the axial CO group remains coordinated upon changing from a CO to an N_2 atmosphere, the concentration of dissolved free CO was progressively decreased by bubbling N_2 through the solution, and cyclic voltammograms were then obtained. Examples of voltammograms after degassing for 1, 4, and 6 min are shown in Figures 7b, 7c, and 7d.

The change in number of processes (from two to one) for electroreduced $Ru_2(F_5ap)_4Cl$ upon going from a CO to an N_2 atmosphere clearly demonstrates the change in coordination which occurs upon formation of the Ru_2^{3+} species. Also, there are no significant differences between the cyclic voltammograms of the electrogenerated (4,0) $Ru_2(F_5ap)_4(CO)$ under CO and cyclic voltammograms obtained after N_2 is bubbled through the solution for 1 min, but changes are clearly seen after N_2 is bubbled for 4 or 6 min. Under the latter conditions, the compound undergoes only a single reduction which is characterized by a reversible electrode process labeled as reaction II in Figure 7c and 7d. The difference in voltammograms as a function of the time of degassing in Figure 7 can be explained by the fact that the reduction of (4,0) $Ru_2(F_5ap)_4(CO)$, i.e., the $Ru_2^{4+/3+}$ process, is accompanied by the uptake of one additional CO molecule when there is CO dissolved in solution. However, Ru_2^{3+} does not bind an additional CO when there is either no CO in solution or a very small amount of dissolved CO in solution, and in these cases a reduction of the Ru_2^{3+} complex to its Ru_2^{2+} form is no longer observed. This experiment also confirms that the CO molecule coordinated to (4,0) $Ru_2(F_5ap)_4(CO)$ does not dissociate from the compound in CH_2Cl_2 solution containing a small amount of CO or no CO at all.

Summary

Eleven diruthenium complexes of the type $Ru_2(L)_4Cl$ which exist in (3,1) and/or (4,0) isomeric form were examined as to their electrochemistry under CO. Each complex was converted to its Ru_2^{2+} form in three well-separated one-electron transfer steps. The Ru_2^{4+} species under CO are proposed to coordinate a single axial CO molecule while both Ru_2^{3+} and Ru_2^{2+} adducts are proposed to contain two CO axial ligands. Both types of carbonyl diruthenium complexes were in-situ electrogenerated in a thin-layer cell and examined as to their UV−visible and FTIR spectroscopic properties. The IR spectra of the Ru_2^{3+}−CO adducts and the UV−visible spectra of the Ru_2^{4+} complex under CO are both isomer dependent, and one can therefore use these results to predict the isomeric form, i.e., (3,1) or (4,0), of diruthenium complexes containing four unsymmetrical ap or substituted ap ligands, especially when attempts to grow a crystal of the Ru_2^{5+} species suitable for single-crystal X-ray diffraction are unsuccessful.

Acknowledgment. The support of the Robert A. Welch Foundation (J.L.B., Grant E-918; K.M.K., Grant E-680) is gratefully acknowledged. We thank Dr. J. D. Korp for performing the X-ray analysis.

Supporting Information Available: X-ray crystallographic files in CIF format for the structural determination of (4,0) $Ru_2(3,4\text{-}F_2ap)_4Cl$ (**3**). Table S1 summarizing the oxidation potentials of $Ru_2(L)_4Cl$ complexes under a CO atmosphere. This material is available free of charge via the Internet at http://pubs.acs.org.

IC035026G